GMR
The Original

INFLUENCE OF Y_2O_3 DOPING ON THE STRUCTURAL, OPTICAL AND BIOLOGICAL PROPERTIES OF SPRAY PYROLYZED MOO_3 THIN FILMS

Sourabh Mohite[1], Supriya Shukla[2], Shrutika Mohite[3], Sharda Gadale[4*]

[1,2,3]Department of Chemistry, Yashwantrao Mohite College of Arts, Science and Commerce, Bharathi Vidyapeeth (Deemed to be University), Maharashtra, India
[4*]Department of Chemistry, Yashwantrao Mohite College of Arts, Science and Commerce, Bharathi Vidyapeeth (Deemed to be University), Maharashtra, India, dagade@rediffmail.com

ABSTRACT
MoO3 nanoparticles doped with Y2O3 could be achieved by using a well-regulated sol-gel method to render its structural, optical, and biomedical properties to be even more useful with defect engineering mediated by rare-earth. The X-ray diffraction has also verified the presence of crystalline orthorhombic MoO3 with effective yttrium incorporation due to the slight changes in peaks and altered crystallite size in absence of secondary impurity phases. Micrographs showed in FESEM all uniformly distributed nanostructures that have a lower agglomeration level and better surface structure when doped. UV-Vis spectroscopy was used to show that there was strong UV absorption with a tuning optical band gap that was explained by lattice distortion and defect level formation. The use of biological evaluation proved a strong antimicrobial effect on bacterial strains of Gram-positive and Gram-negative and confirmed that efficacy of membrane disruption and microbial inhibition by Reactive Oxygen Species (ROS). Antioxidant tests indicated a high free-radical scavenging capacity, and the result also showed that there was a redox-active surface behavior. Moreover, the highest performance of NO2 was produced by the 0.1 M Y2O3-doped MoO3 thin film, which showed desirable selectivity, response size and sensitivity at the optimum operating temperature relative to the low concentrations of precursors (0.025 M and 0.05 M). Comprehensively, yttrium doping provided a substantial impact on crystallinity, surface defects, and biological performance, making Y2O3 doped MoO3 nanoparticles to be promising multifunctional nanomaterials in antimicrobial.

GRAPHICAL ABSTRACT:

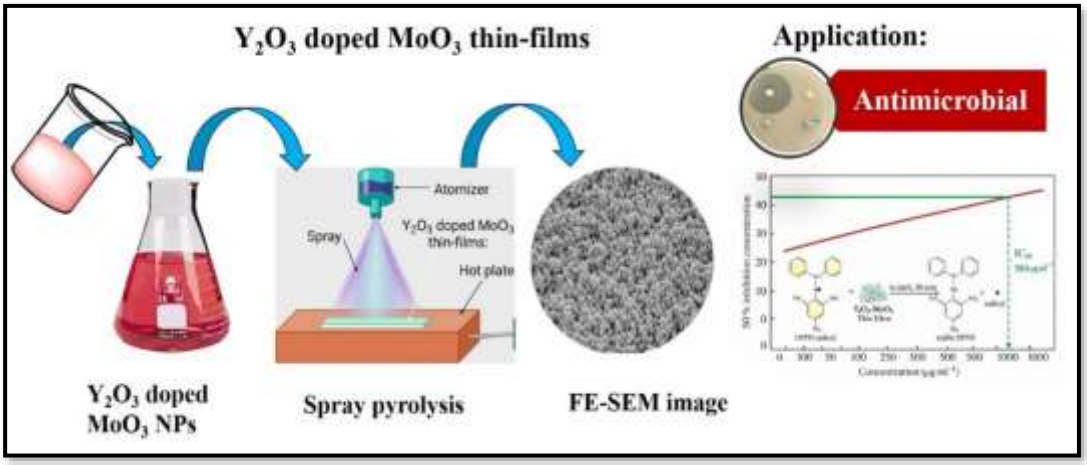

KEYWORDS: Y2O3 doped MoO3, spray pyrolysis synthesis, rare-earth doping, oxygen vacancies, defect engineering, antimicrobial activity, antioxidant activity

INTRODUCTION

The threatening increase in Antimicrobial Resistance (AMR) is an alarming phenomenon and has become one of the main global public-health challenges in the 21st century. According to data published by World Health Organization (WHO), millions of deaths per year may be caused by drug-resistant infections unless new treatment options are created. The decreasing activity of traditional antibiotics, as well as the slow pace of the discovery of new materials that can eliminate microbial pathogens through non-traditional routes [1]. In addition to bacterial resistance, increasing fungal infection and diseases-related challenges associated with oxidative stress also highlight the necessity with antimicrobial, antioxidant, and possibly, anti-cancer properties. Therefore, metal oxide nanomaterials have received great scientific interest due to

their remarkable unique physicochemical characteristics. In contrast to traditional antibiotics which exhibit uniform effects on particular biochemical pathways, metal oxides display broad-spectrum action with multi-target effects, and thus the probability of the development of resistance is minimized [2].

As evidenced in several studies, such as Jones et al., have shown that metal oxide surfaces exhibit long-term antimicrobial activity because of intrinsic catalytic and redox characteristics of metallic oxide. Within the scientific community, Molybdenum trioxide (MoO3) is prominently emerging and has attracted by the growing scientist [3]. Due to its high oxidation state, strong surface acidity and overcoated layer of orthorhombic crystal structure. Investigations that have been conducted before have revealed that MoO3 has the capacity to mediate bactericidal effects by producing molybdic acid in an aqueous solution, which subsequently suppress microbial proliferation. Indicatively, Martínez et al. had found that MoO3-based materials significantly decreased the viability of Staphylococcus aureus and Escherichia coli by facilitating the proton mediated membrane destabilization. Moreover, Singh et al., demonstrated that morphology-related antibacterial behavior in MoO3 nanorods, which suggests that the crystal orientation, surface defects, and particle size have a critical role on biological performance [4, 5].

In spite of these promising findings which has been reported, most of the studies have focused on MoO3 nanoparticles, bulk or composite matrices. Particularly, in the biomedical context, thin-film architectures, and more recently those created by scalable industrially viable processes, are relatively underutilized [6]. There are several benefits of the thin films, which include uniform and complete coverage of the surface, strong adhesion with substrates, precise thickness, and can be used in medical coating and device combination. However, systematic studies that provide a correlation between structural, optical, and surface chemical properties of MoO3 thin films and their multifunctional biological performances are few [7]. It is generally recognized that doping is a powerful technique to alter the electronic structure, defect concentration, crystallinity, and surface chemistry of metal oxides. Capable of changing lattice parameters, facilitating charge carrier separation, and increasing surface reactivity, rare-earth dopants have demonstrated to be useful in nanoparticles, especially yttrium (Y3+). Yttrium oxide (Y2O3) is described as highly thermal conducting, favorable dielectric and biocompatible [8]. The experimental data of Y-doped ZnO and TiO2 systems shows that they exhibit better antimicrobial and photocatalytic activities, which can be explained by defect engineering and optimal electron-hole separation. Recent studies, on the contrary, have focused less on the use of yttrium in MoO3 thin films particularly in terms of the overall impact on structural development, band-gap development, and bioreactivity [10].

Based on these research gaps, the current research attempts to bridge these gaps by synthesizing Y-doped MoO3 thin films through a spray pyrolysis method and systematically exploring its physicochemical and biomedical characteristics. Examination of the structural features entails X-ray diffraction (XRD) to determine the crystallinity and purity of its phases. The surface morphology and microstructure are studied with the help of field-emission scanning electron microscopy (FESEM), chemical bonding and functional groups are analyzed using Fourier transform infrared spectroscopy (FTIR) and the estimation of optical properties and band-gap is done based on UV-visible spectroscopy. Besides, the bioactivity assessment of the prepared films is also done using antimicrobial, and antioxidant studies to determine a global structure-activity relationship. The proposed research will focus on the enhancement of next-generation biomedical coatings that can overcome the current antimicrobial and oxidative-stress challenges by the integration of controlled yttrium doping with thin-film engineering and multifunctional biological evaluation.

Experimental:

Materials:

All the chemicals used in this work were of analytical grade and were used without further purification. Ammonium heptamolybdate tetrahydrate (NH4)6Mo7O24.4H2O (99% purity) was chosen as the molybdenum precursor and the yttrium nitrate hexahydrate Y(NO3)3·6H2O (99.9% purity) as a dopant precursor, was obtained through Sigma-Aldrich (Mumbai, India). In case of the biological assays, HiMedia Laboratories Pvt. Ltd. Bought Muller-Hinton agar (MHA), and potato dextrose agar (PDA). The assessments of antioxidant activity were compared against 2,2-diphenyl-1-picrylhydrazyl (DPPH) radical scavenging activity, and ascorbic acid obtained at Merck (Mumbai, India).

Microorganisms:

The antimicrobial performance of the Y2O3 doped MoO3 thin films was evaluated against a standard reference panel of microbial strains. The organisms that were used in the tests included Staphylococcus aureus (ATCC 6538) which is a Gram-positive cocci, Escherichia coli (ATCC 8739), Bacillus subtilis (ATCC 6633) Gram-positive rod, and Pseudomonas aeruginosa (ATCC 15442) that are Gram-negative bacilli and Candida albicans (ATCC 14053) which is a common pathogenic yeast. All cultures were prepared in lyophilate form of authenticated repositories and reactivated through normal laboratory conditions before being experimented. The experiment processes were carried out under aseptic conditions to ensure the reproducibility and reliability of the biological analyses.

Synthesis of thin-film:

Thin layer of Y2O3 doped MoO3 were sprayed on clean glass surfaces using a spray pyrolysis methodology shown in Figure 1. A clear solution of molybdenum precursors was obtained by dissolving aqueous solution of (NH4)6Mo7O24 .4H2O, which was subjected to constant magnetic stirring. To ensure controlled incorporation of yttrium, Y(NO3)3·6H2 O was used as the source of dopant at 0.025M, 0.05M, and 0.1M levels [15]. The precursor solution was atomized and transported to a heated substrate through compressed air which acted as a carrier gas. The nozzle substrate distance was kept at a relatively constant of about 20 cm to guarantee uniform deposition. Droplet sprayed on the heated substrate were subjected to rapid solvent evaporation then subjected to thermal decomposition, to form Y2O3 doped MoO3 thin films.

The films were fabricated under the same deposition conditions to determine the effect of yttrium concentration on the film properties systematically. The samples were allowed to cool to room temperature after the deposition and to be post-annealed to increase crystallinity and phase stability [16-18].

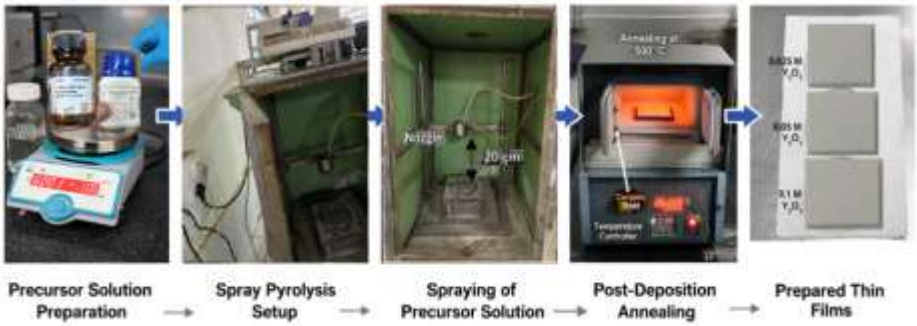

Figure 1: Synthesis of Y2O3 doped MoO3 thin-films

Characterization:
The crystallographic structure and phase purity of Y2O3 doped MoO3 thin films were evaluated by the XRD technique using a Rigaku MiniFlex 600 diffractometer equipped with CuKα radiation source (1.5406 Å), operated at 40 kV and 30 mA, at a 2θ range of 10-80ºC. These diffraction patterns were then used to calculate the crystallographic phase, lattice parameters and crystallite size based on the Debye–Scherrer relation. Field-emission scanning electron microscopy (FESEM) using a JEOL JSM-7600F microscope, operated at an accelerating voltage 5-15 kV, to investigate the surface morphology and microstructural properties of the deposited films [21-26]. Micrographs of high-resolution revealed grain-distribution, surface uniformity and continuity of the film. The spectra of Fourier-transform spectroscopy (FTIR) were recorded in the range of 400-4000 cm-1 to determine presence of typical vibrational modes and the occurrence of MoO3 and Y2O3 bonding interactions in the thin films. Their optical properties were examined though the use of UV prove 1800, Shimadzu, UV-visible spectroscopy between 200-800 nm at ambient temperature with a spectral resolution of 1 nm. Tauc plots based on the data on the absorption were used to extract the optical band-gap energy [40-45].

Antimicrobial Activity:
To test the antibacterial and antifungal capabilities of the produced Y2O3 doped MoO3 thin films, the agar well diffusion test was carried out according to the principles of the Clinical and Laboratory Standards Institute (CLSI). The standard microbial strains that were used included Staphylococcus aureus (ATCC 6538), Bacillus subtilis (ATCC 6633), Escherichia coli (ATCC 8739), Pseudomonas aeruginosa (ATCC 15442), and the fungal isolate Candida albicans (ATCC 14053). Bacterial cultures were incubated in a Muller-Hinton broth at 37ºC during 18 to 24 hours, and the fungal organism grew in a potato dextrose broth at 28ºC in 24 to 48 hours in order to get actively growing inoculum. The turbidity of the individual microbial suspensions was zeroed to the 0.5 McFarland standard, which is approximately 1X108 CFU ml-1 of bacterial strains [27]. Sterile Muller-Hinton agar plates (bacteria) and potato dextrose agar plates (fungi) were inoculated evenly with 100 µl of the standardized microbial suspension by placing the sterile cotton swabs. Agar medium was aseptically prepared with wells of 6 mm diameter. Aliquots (100 µl) of Y2O3 doped MoO3 samples (0.025M, 0.05M, and 0.1M, which corresponds to 5 mg/ml-1 and 10 mg/ml-1) were added to the corresponding wells. The negative control was dimethyl sulfoxide (DMSO), positive controls were Streptomycin (in case of bacterial strains) and Fluconazole (in the case of the fungal strain) [28]. After 20 minutes incubation at ambient temperature, the plates were incubated at 37ºC (bacteria) and 28ºC (fungi) respectively. The measurement of antimicrobial efficacy was achieved through measuring the diameter of the inhibition zone (mm) around every well. The experiments were performed triplicate and all findings were given as the average standard deviation [29].

Antioxidant Activity:
Free radical scavenging activity of the prepared Y2O3 doped MoO3 thin films was analyzed using the 2,2-diphenyl-1-picrylhydrazyl (DPPH) assay. A 0.1mM of newly prepared DPPH solution in methanol was prepared and it was stored away to prevent photolytic. Three different concentrates of the synthesized thin-films (0.025M, 0.05M, and 0.1M) have been prepared and then used to carry out the analysis. Each sample concentration was added to an aliquot of 1.6 ml combined with 2.4 ml of DPPH solution. The corresponding reaction mixtures were then vortexed and left at ambient temperature in the dark over a period of 30 min in order to procure full interaction between DPPH radicals and the antioxidant constituents. The spectrophotometric absorbance of the end solution was determined on the basis of a UV-visible spectrophotometer at 517 nm, where methanol of DPPH is the negative control. Ascorbic acid was used as the standard antioxidant. All measurements were done thrice and the values were expressed as mean ± SD. The DPPH radical scavenging activity was determined as a percent of the following formula:

$$Scavenging\ activity\ (\%) = \frac{\mathrm{A0} - \mathrm{A1}}{\mathrm{A0}}\ X\ 100$$

In which, A0 represents the control, and A1 represents the absorbance of the test sample. IC50 was calculated by applying percentage inhibition vs concentration and calculating the concentration necessary to remove 50% of DPPH radicals.

RESULT AND DISCUSSION

Mechanism of Y2O3 Doping in MoO3 thin-film:

The addition of Y3+ ions into the lattice of MoO3 can significantly change the structural and electrical characteristics of the thin film. Orthorhombic MoO3 is comprised of MoO6 octahedra, which are distorted with Mo majorly having a +6 oxidation state. Doping of Y3+ ions replace the Mo6+ sites are substituted by Y3+ ions, thus causing lattice deformation due to the difference in ionic radii (Y3+ > Mo6+). Due to the low valence state of Y3+ compared to Mo6+, this charge compensation is accomplished by oxygen vacancy formation and partial reduction of Mo6+ to Mo5+ (Fig. 2). The defect reaction may be expressed as follows:

$$Y_2O_3 \rightarrow 2Y^{3+} + 3O^{2-}$$

$$Y^{3+} + Mo^{6+} \rightarrow Y\_Mo + Mo^{5+} + V_0$$

The vacancies generated serve as donor sites thus increasing the carrier concentration and electrical conductivity. Those flaws create localized states in the band gap causing a slight narrowing of the band gap and enhanced charge transfer dynamics. Moreover, the existence of Mo5+/Mo6+ redox couple enhances electron transfer, which facilitates the production of reactive oxygen species (ROS) in physiological conditions. The increased ROS generation is involved in oxidative stress-induced apoptosis in cancer cells. As a result, Y2O3 doping enhances structural disorder, defect density, and redox activity of the MoO3 thin film, which boosts bio-functional performance of the materials.

FESEM Analysis:

FESEM was utilized to investigate the surface morphology of Y2O3 doped MoO3 thin films at precursor molarities of 0.025M, 0.05M, and 0.1M (Fig. 3). The micrographs display the strong effect of the precursor concentration on the uniformity of the film, grain size, and compactness of the surfaces. Films at 0.025M have a fairly uniform and loosely packed structure containing fine grains and visible intergranular voids. This decrease in precursor concentration probably leads to a decrease in the nucleation density and retards growth kinetics to yield more porous thin-film with minimal coalescence between grains. This type of morphology is normally related to deposition under control and gradual film formation. When the precursor molarity is increased to 0.05M, the coverage of the surface and the connection between the grains are improved [21]. The films exhibit a greater microstructure and smaller void spaces and start to show partially bended grains, which show an increased nucleation density and faster lateral grain growth. Higher concentration of ion facilitates the nucleation through supersaturation creating more continuous film. Conversely, the 0.1M films exhibit a highly compact and densely packed morphology with pronounced agglomeration of the grains with diminished porosity. The increased growth kinetics and rapid nucleation at high precursor concentration enhance the process of grain coalescence as well as vertical thickening of the film. This leads to better structural compactness and better film continuity that could have great impact on electrical and optical properties [22]. In general, FESEM analysis reveals that both Y2O3 and MoO3 thin-films exhibit improved grain density and film compactness with an increasing in precursor molarity. The recorded morphological development of porous microstructures at low molarity concentration to densely packed films at high concentration level to densely packed films at high concentration reveal the importance of precursor concentration in controlling the nucleation-growth dynamics in the formation of thin films.

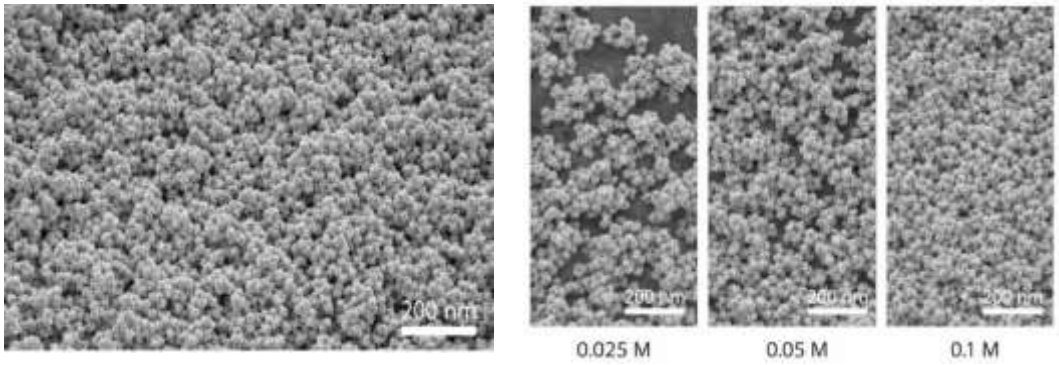

Figure 2: Surface Morphology of Y2O3 doped MoO3 thin-films

XRD Analysis:

There are noticeable reflections at 2θ ≈ 24.55°, 30.24°, 36°, and 48.9° in the X-ray diffraction (XRD) pattern (Figure 4). The orthorhombic α-MoO_3 phase (JCPDS No. 05-0508) is thought to be responsible for the peak at 24.55°, which corresponds to a slightly displaced (110)/(040) plane reflection and may be caused by lattice distortion brought on by yttrium inclusion. The orthorhombic structure is retained at higher-order reflections, as evidenced by the peak at 36° that corresponds to the (121) plane and the peak at 48.9° that is attributed to the (221) plane of α-MoO_3. The peak at 30.24° closely matches the Y_2O_3 major diffraction peak (JCPDS No. 41-1105), indicating the existence of species related to yttrium [22-30].

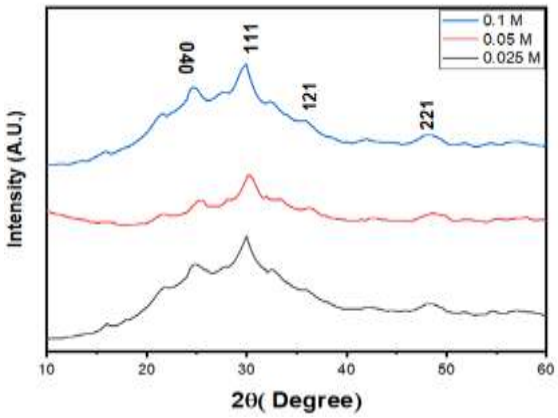

Figure 3: Diffraction Patterns of Y2O3 doped MoO3 thin-films

UV-Visible Analysis:
The optical band gap of yttrium oxide (Y_2O_3) doped molybdenum oxide (MoO_3) thin films was determined from UV–Vis absorption spectra using the Tauc relation, which describes the dependence of the absorption coefficient (α) on photon energy (hν):
$(\alpha h\nu)n = A(h\nu - Eg)$
where hν is the photon energy,
Eg is the optical band gap
A is a constant, and n=1/2 for indirect allowed transitions. The band gap values were estimated by extrapolating the linear region of the $(\alpha h\nu)2$versus hν plot to the energy axis (figure 5). The calculated optical band gap values for Y_2O_3-doped MoO_3 thin films at different precursor concentrations are summarized below [21-26].

Y_2O_3 concentration	Band gap (Eg)
0.025 M	3.47 eV
0.05 M	3.21 eV
0.1 M	3.13 eV

For films made with precursor concentrations of 0.025 M, 0.05 M, and 0.1 M, the computed band gap values were 3.47 eV, 3.21 eV, and 3.13 eV respectively. The findings clearly show that the band gap energy gradually decreases as the concentration of Y_2O_3 increases.
The introduction of Y^{3+} ions into the MoO_3 lattice, which provides defect states and oxygen vacancies that form extra energy levels inside the band structure, may be responsible for this decrease in band gap. By facilitating electronic transitions at lower photon energy, these localized states shrink the effective band gap. The development of impurity levels and band tailing effects in the doped films is further supported by the red shift in the absorption edge with increasing dopant concentration [27-28].

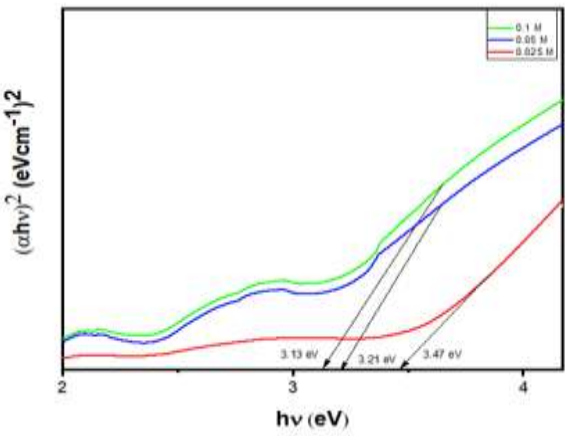

Figure 4: UV-Visible absorption data of Y2O3 doped MoO3 thin-films

Antimicrobial Analysis:
The antimicrobial activity of MoO3 thin-films with the doped Y2O3 were investigated using the agar well diffusion method at the concentrations of 0.025M, 0.05M, and 0.1M of the precursor. Antibacterial studies were conducted on the isolates of Staphylococcus aureus (ATCC 6538), Bacillus subtilis (ATCC 6633), Escherichia coli (ATCC 8739), and Pseudomonas aeruginosa (ATCC 15442); antifungal against Candida albicans (ATCC 14053). Streptomycin and

fluconazole, were used as reference agents, respectively. The data show in Table 1 & Table 2, that the antimicrobial effect is variable with the concentration of dopant and applied dosage (5 mg and 10 mg). The 0.025M doped films showed modest antibacterial effects with an inhibition zone of 1-3 mm with 5 mg and a small increment to 10 mm with the maximum antibacterial effect with 10 mg on Bacillus subtilis. In comparison, the 0.05M film did not have a significant activity, with an inhibition zone of 1-2 mm on most of the bacterial strains regardless of dosage. In contrast, MoO3 film doped with 0.1M Y2O3 had significantly better antibacterial activity. Inhibition zones observed at 5 and 10 mg were 4-5 mm and 8-11 mm respectively, the most sensitive strain was P. aeruginosa and was capable of achieving an inhibition region of 11 mm in diameter. Despite the fact that these diameters are still poorer than streptomycin-produced diameters (27-32 mm), the results confirm a dopant-concentration-dependent increase in antibacterial activity. The doped films (0.025M and 0.05M) showed inhibited growth (25 mm), and the 0.1M film recorded strong antifungal activity, with a 16 mm inhibition area at 5 mg and 22 mm at 10 mg. These diameters are low compared to the reference fluconazole (30 mm), the enhanced performance of the 0.1M film supports its capability as an antifungal agent [30-33].

Table 1: Zone of Inhibition by Antimicrobial activity for Y2O3 + MoO3

Microorganism / Sample	Y2O3 + MoO3 0.025M	Y2O3 + MoO3 0.05M	Y2O3 + MoO3 0.1M
E.coli			
S.aureus			
Bacillus			
Pseudomonas			
C.albicans			

Table 2: Antimicrobial activity detail of Y2O3 doped MoO3 thin-film effects on various concentrations (0.025, 0.05, and 0.1M) with different loadings (5 mg and 10 mg)

Sr.	Sample	Concentration	Zone of Inhibition

No.			E.coli	S.aureus	Bacillus	Pseudomonas	C.albicans
1	Control	-	-	-	-	-	-
2	Std. Streptomycin	-	29	27	30	32	30
3	Y2O3 + MoO3 0.025M	5 mg	01	01	03	02	02
		10 mg	03	03	10	04	04
4	Y2O3 + MoO3 0.05M	5 mg	01	01	01	01	03
		10 mg	02	02	02	02	05
5	Y2O3 + MoO3 0.1M	5 mg	04	05	04	05	16
		10 mg	09	08	09	11	22

Mechanism of Antimicrobial Action:

The antimicrobial activity of the MoO3 thin-film doped with Y2O3 may be attributed to their semiconducting properties and surface reactivity. The band gap of MoO3 is large and this means that on proper activation conditions, the electron and hole pairs are produced. These carrier charges help in the generation of reactive oxygen species (ROS), such as hydroxyl radicals and superoxide anions (Fig. 6). The resultant ROS induce oxidative stress, which leads to lipid peroxidation, denaturation of proteins and damage of DNA in the microbial cells [31]. Furthermore, the substitution of Y2O3 can modify the architecture of the surface defects and optimize the density of the oxygen vacancies, which can boost the effectiveness of ROS formation. Membrane permeability continues to be further hampered by the interaction of the released metal ions and negatively charged cell membranes of microbes further destabilizing cellular metabolism. Observed differences in susceptibility may therefore be explained by structural differences between gram-positive and gram-negative bacteria [32].

High antimicrobial activity exhibited by the 0.1M sample could be attributed to the optimum level of crystallinity, increased surface area and high charge separation efficiency to achieve effective microbial inhibition. Concentrations (0.025M, 0.05M, and 0.1M) are expected to have relatively poor morphological and defect properties, leading to reduced antimicrobial activity. Altogether, the results show that an increase in Y2O3 doping concentration has a significant positive effect on the antimicrobial properties of MoO3 thin films with the most potent antibacterial and antifungal action among the analyzed compositions [33].

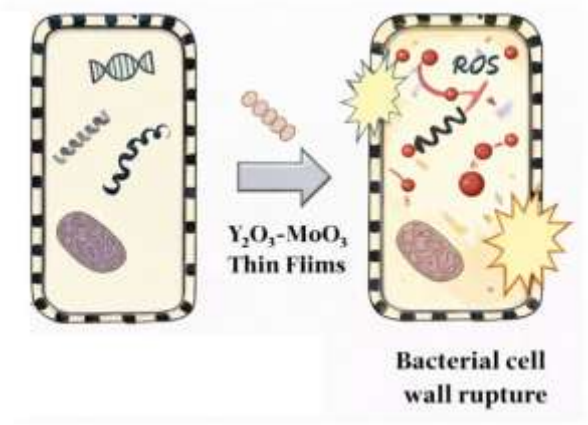

Figure 6: Mechanism of Antimicrobial action of Y2O3 doped MoO3 thin-films

Antioxidant Analysis:

To determine the antioxidant activity of Y2O3 doped MoO3 thin-films, prepared at 0.025M, 0.05M, and 0.1M of the precursors, was measured using the DPPH free radical scavenging assay, which was carried on 96 plates of microplates. Increasing sample concentration had a progressive effect on the absorbance at 517 nm, which supported the ability of the films to neutralize the action of DPPH radicals in a concentration-dependent process. The IC50 value of thin-films was obtained to be 384 µg ml^{-1}, reflecting a medium free radical scavenging ability (43%), shown in Figure 7. Ascorbic acid which was used to act as the reference antioxidant, showed a high scavenging activity, with the percentage inhibition of 76.80%, 81.70%, and 97.23% at concentrations of 250, 500, and 1000 µg ml-1, respectively. Conversely, the resulting thin-films had relatively average radical-scavenging capacity [34, 35]. At 250, 500, and 1000 µg ml-1 the 0.025M sample displayed an inhibitory efficiency of 21.50%, 28.19% and 29.97%, respectively, showing a gradual increase in the concentration (Table 3). The film (0.05M) recorded a relatively lower activity of 250 µg ml-1 (11.03%), then 21.97%,

and 27.24% at 500 µg ml-1 and 1000 µg ml-1. The measured antioxidant performance was moderate with inhibition values of 15.76%, 24.67%, and 22.82% at concentrations of 0.1M respectively. All sample shared the same concentration dependent free radical scavenging activity; the 0.025M and 0.1M films were relatively better performing among the investigated compositions. This is probably the antioxidant effect of transferring an electron between the metal-oxide surface and the DPPH radical with the aid of surface defects and oxygen vacancy created through Y2O3 doping [36-38]. These results indicate that the MoO3 thin-films with Y2O3 have moderate antioxidant properties and that such a property can be beneficial in biomedical and protective-coating studies.

Table 3: Effects of samples by using Antioxidant activity by DPPH (96 well method)

Antioxidant Activity by DPPH (96 well method)						
Sample Code	Concentration	Absorbance			Mean	% Inhibition
Control		0.985	0.988	0.989	0.987	-
Standard Ascorbic acid	250	0.235	0.224	0.228	0.229	76.80
	500	0.189	0.178	0.175	0.180	81.70
	1000	0.025	0.028	0.029	0.027	97.23
Y2O3 + MoO3 0.025M	250	0.789	0.758	0.778	0.775	21.50
	500	0.725	0.724	0.678	0.709	28.19
	1000	0.687	0.689	0.698	0.691	29.97
Y2O3 + MoO3 0.05M	250	0.879	0.877	0.879	0.878	11.03
	500	0.768	0.775	0.768	0.770	21.97
	1000	0.723	0.721	0.711	0.718	27.24
Y2O3 + MoO3 0.1M	250	0.824	0.838	0.833	0.831	15.76
	500	0.778	0.775	0.678	0.743	24.67
	1000	0.762	0.772	0.752	0.762	22.82

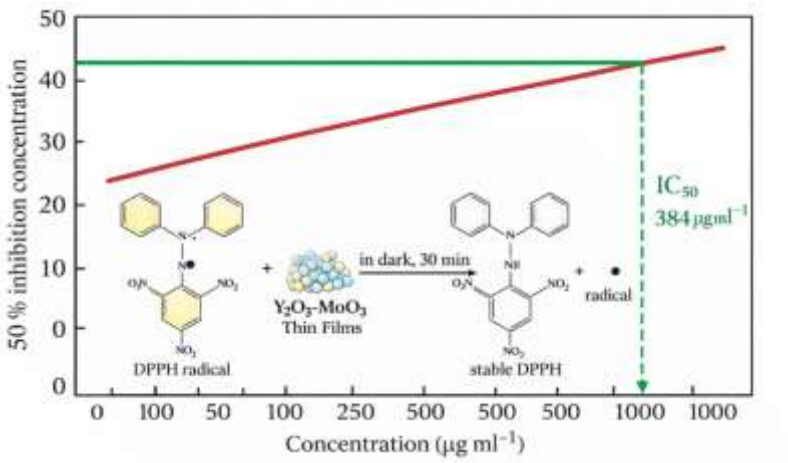

Figure 7: Antioxidant Activity of Y2O3 doped MoO3 thin-films

CONCLUSION

Within the current study, MoO3 nanoparticles doped with Y2O3 were effectively prepared using a controlled sol-gel methodology, indicating a dependable and validated technology of synthesizing structurally stable rare-earth-modified metal oxide nanostructures. XRD analysis revealed that slightly amorphous orthorhombic MoO3 was formed and slight change of peak and crystalline size showed that yttrium was successfully incorporated into the lattice. FESEM showed that nanostructures were uniformly distributed and agglomeration was reduced and surface texture was modified on doping, indicating enhanced surface reactivity. UV-VIS spectroscopy revealed a high adsorption in the UV region which with adjustable band gap the energy-level adjustment caused by defects and interaction of rare-earths within the MoO3 medium.

It was determined that the engineered nanoparticles had significant antimicrobial activity against Gram-positive and Gram-negative strains, which could be linked to membrane disruption, ROS generation, and metal ion interaction with microbial proteins and DNA, which have been widely reported on metal oxide nanoparticles via biological studies. The antioxidant test also revealed significant levels of free radical scavenging activity, which suggests redox-modulating properties associated with oxidation holes and surface-active sites.

In general, the synergistic combination of rare-earth doping increased crystallinity, defect density, surface chemistry and electronic structure, and all these factors contributed to the enhanced multifunctional performance. These findings confirmed that Y2O3 doped MoO3 nanoparticles as potentially useful in biomedical and antimicrobial agents and indicate that defect engineering regulating the physicochemical and biological properties could be significant.

Conflict of Interest:
The authors declare that they have no known financial conflict of interest or any personal affiliations that could be interpreted to influence the study that is conducted in this paper.

REFERENCES

1. A. Salim, S. Sadhasivam, Nano and Medical Materials, 3,1(2023); https://doi.org/10.59400/nmm.v3i1.73
2. C.Zollfrank, K. Gutbrod, P.Wechsler, J.P Guggenbichler, Materials Science and Engineering, 32(1), 47-54(2012) https://doi.org/10.1016/j.msec.2011.09.010
3. N.tijani, O.Akintayo, M.popoola, H.kim, S.Adewinbi, Inorganic Chemistry Communications 171, 113610(2025); https://www.sciencedirect.com/science/article/abs/pii/S1387700324016009
4. M. Ikram, I.Atiq, A. Rafiq Butt, I. Shahzadi, A. Ul-Hamid, A.Haider, W. Nabgan, F Medina, Front Chem. 9;11:1191849 (2023); https://doi.org/10.3389/fchem.2023.1191849
5. D. V. Ahire, S,D.Shinde, K.K. Thakuar, G.H. Jain, Paradigm, 5(3), (2012); https://sciendo.com/article/10.21307/ijssis-2017-497
6. V. Ganesh, I.S.Yahia, Optical Materials, 144,114280, (2023); https://www.sciencedirect.com/science/article/abs/pii/S0925346723008522
7. R.Balaji, P.Seenuvasakumaran, R.Anandhi, A.Vinodhini, Materials science, 326, 119188 (2026); https://www.sciencedirect.com/science/article/abs/pii/S0921510726000115
8. Min Hu, Chenwen Li, Xin Li, Nanomed Biotechnol, 46(6):1248-1257(2018); https://doi.org/10.1080/21691401.2017.1366339
9. K. Krishnamoorthy, M. Premanathan, M.Veerapandian, S J Kim, Nanotechnology. 20148;25(31):315101,(2014); https://pubmed.ncbi.nlm.nih.gov/25030310/
10. E. Lopes, S. Piçarra, P.LAlmeida, H. Lencastre, J .Med, Microbiol. 67(8):1042-1046,(2018); https://pubmed.ncbi.nlm.nih.gov/25030310/
11. P.Bharathidasan, M.Surya, P.Geetha Sravanthy, M.Saravanan, National Library of Medicine, 16(3),56760 (2025); https://pubmed.ncbi.nlm.nih.gov/38650815/
12. Y.Gilad Barzilay, A.Yucknovsky, N.Amdursky, Transfer Mechanism Nano Lett. 24(6):1936-1943(2024); https://pubmed.ncbi.nlm.nih.gov/38289664/
13. EY.Ahn, H.Jin, Y.Park, Mater Sci Eng 101:204-216 (2019); https://pubmed.ncbi.nlm.nih.gov/31029313/
14. W.Huang, Y.Zhou, Y.Deng, , National Library of Medicine, 20(6):4347-4350 (2018); https://pubmed.ncbi.nlm.nih.gov/29368000/
15. J.Cho, S.Hwang, K.DH, S.Chung, Materials (Basel). 12(20):3423 (2019); . https://pubmed.ncbi.nlm.nih.gov/29368000/
16. FH.Alkallas, Ben Gouider, A.Trabelsi, M.Shkir, S. AlFaify, Nanomaterials 12(16), 2797(2022); https://pubmed.ncbi.nlm.nih.gov/36014662/
17. A.Mathi Vathani, S.Dhanalakshmi, N.Jeyakumaran, N.Prithivikumaran., Fabrication of Al- J Nanosci Nanotechnol. 20(5) 2887-2892 (2020); https://pubmed.ncbi.nlm.nih.gov/31635625/
18. P.Bancheva-Koleva, V.Zhelev, P.Petkov, T.Petkova, Materials (Basel). 17(9):2164(2024; https://pubmed.ncbi.nlm.nih.gov/38730970/
19. J,Sydorenko, M.Krunks, A.Katerski, R.Grzibovskis, A.Vembris, A.Mere, N.Spalatu, RSC Adv. 2024 14(28):19648-19657(2024); https://pubmed.ncbi.nlm.nih.gov/38899031/
20. I.Dundar,M. Krichevskaya, A.Katerski, R Soc Open Sci. 6(2):181578(2019); https://pubmed.ncbi.nlm.nih.gov/30891278/
21. TC Lin, JY Wu, AJJ Mendez, N.Salazar , HL Hsu, Materials (Basel),17(15):3677(2024); https://pubmed.ncbi.nlm.nih.gov/39124342/
22. L HE, DRT Zahn, TI Madeira, National Library of Medicine,16(15):5494.(2023); https://pubmed.ncbi.nlm.nih.gov/37570199/
23. M. Khan, GA.Nowsherwan, R.Ali, M.Ahmed, N.Anwar, S.Riaz, A.Farooq, SS Hu. National Library of Medicine 28(24):7963 (2023); https://pubmed.ncbi.nlm.nih.gov/38138453/
24. G.Evmenenko, TT Fister, FC Castro, X.Chen, B. Lee, DB. Buchholz ,VP Dravid, P.Fenter ,Physical Chemistry chemical Physics 21(1):8897-8905(2019); https://pubmed.ncbi.nlm.nih.gov/30982834/
25. A. Phili, R. Ghiyasi, M.Karppinen, National Library of Medicine 26(11):3214 (2021); https://pubmed.ncbi.nlm.nih.gov/34072008/
26. SJ Patil, AC Lokhande, DW Lee, JH Kim, CD Lokhande, J Colloid Interface 490:147-153 (2017); https://pubmed.ncbi.nlm.nih.gov/27898333/
27. J.Göransson, M.Sundqvist, E. Ghaderi, JG Lisby, Y.Molin, E.Eriksson, S.Carlsson, A.Cederlöf, L.Ellis, J.Melin, National Library of Medicine 61(3):0152522 (2023); https://pubmed.ncbi.nlm.nih.gov/36852983/
28. I.Kara, AIR Hafedh, NKH Alhusseinawi, AF Kayış AF, O. Yalçınkaya, BC.Acar, Z.Yuksekdag , Y.Ozen, O.Gençyılmaz, Ec Ozkan . Microsc Res Tech, 87(12):2915-2928 (2024); https://pubmed.ncbi.nlm.nih.gov/39051772/
29. BF Finina, AK Mersha, RSC Adv. 14(8):5290-5308.(2024). https://pubmed.ncbi.nlm.nih.gov/38357038/
30. M. Faya, HA. Hazzah, CA Omolo, N.Agrawal, P.Walvekar, C.Mocktar, B. Nkambule, S.Rambharose, F.Albericio, Amino Acids. 52(10):1439-1457(2020); https://pubmed.ncbi.nlm.nih.gov/33074344/
31. D.Predoi, CL Popa , P.Chapon, A.Groza, SL Iconaru. Materials (Basel).16;9(9):778(2016); https://pubmed.ncbi.nlm.nih.gov/28773899/

32. T.Yan, F.Li, J.Li, F.Chen, Microbiol Spectr. 9(3):0136421(2021); https://pubmed.ncbi.nlm.nih.gov/34908455/
33. S. Shukla, S. Salunkhe, V. Raut, S.Mohite, K.Sharma, S. Gadale, Asian Journal of Chemistry 38, 425-433(2026); https://doi.org/10.14233/ajchem.2026.34808
34. VG Prabitha, J. Sahadevan, M.Madhavan, SF Muthu, I.Kim, TK Sudheer, P.Sivaprakash, Discov Nono 18(1):155(2023);https://pubmed.ncbi.nlm.nih.gov/38108894/
35. A.Khurana,P. Anchi, P. Allawadhi, V.Kumar, N.Sayed, G.Packirisamy, C. Godugu Nanomedicine. 54-65.(2019); https://pubmed.ncbi.nlm.nih.gov/30851439/
36. R. Prior,X.Wu, K.Schaich, Agric Food Chem 53(10):4290-302 (2005); https://pubmed.ncbi.nlm.nih.gov/15884874/
37. G.Shi, S.Lan, Q.Zhang, J.Wang, F.Shu, Z.Hao ,T. Chen, M.Zhu , R.Chen , J.Chen , Z.Wu, Biomaterials 315:122909 (2025); https://pubmed.ncbi.nlm.nih.gov/39471714/
38. JH. Joun , L.Li, J An, J.Jang, YK Oh, CS. Lim, YS. Kim, K.Choi, JP Lee, J.Lee, PLoS One. 19(8):0306025(2024);. https://pubmed.ncbi.nlm.nih.gov/39088565/
39. Frontiers Editorial Office, Front Chem.;11:1285225(2023); https://pubmed.ncbi.nlm.nih.gov/37731453/
40. S.Duangmanee,Y. Poo-Arporn, P.Janphuang,P. Leuasoongnoen, S.Tonlublao, P.Kamonpha , N.Saengchai, N.Chanlek, C.Saisombat , P.Kidkhunthod , RP.Poo-Arporn, Nanomaterials (Basel), 12(8):1285 (2022); https://pubmed.ncbi.nlm.nih.gov/35457993/
41. I.Dascalu, C.Hornoiu, JM.Calderon Moreno,P. Osiceanu, S.Somacescu, Gels.9(8):638(2023); https://pubmed.ncbi.nlm.nih.gov/37623092/
42. Y.Yang, B.Maeng, DG Jung, J.Lee , Y.Kim, J.Kwon ,Hk An, D.Jung, Nanomaterials (Basel)12(18):3227(2022); https://pubmed.ncbi.nlm.nih.gov/36145014/
43. D.Bej, N.Chattaraj, R.Sahu, Rev Sci Instrum, 95(3):035106(2024); https://pubmed.ncbi.nlm.nih.gov/38441427/
44. KK.Sharma, D.Sharma ,DW. Boukhvalov, U.Khandelwal , P.Nukala , N.Bhat, R.Karuppannan, National Library of Medicine,17(1):82.(2025); https://pubmed.ncbi.nlm.nih.gov/41345090/
45. M.Proença, MS.Rodrigues, DIMeira, MCR Castro, PV.Rodrigues, AV.Machado, E.Alves, NP.Barradas, J. Borges, Sensors (Basel),22(18):7043.(2022); https://pubmed.ncbi.nlm.nih.gov/36146392/